Learning to self-fold at a bifurcation

Chukwunonso Arinze, Menachem Stern, Sidney R. Nagel, and Arvind Murugan

Learning to self-fold at a bifurcation

Chukwunonso Arinze[1], Menachem Stern[2], Sidney R. Nagel[1], Arvind Murugan[11, 2]

[1]*Department of Physics, University of Chicago, Chicago, IL 60637*
[2]*Department of Physics and Astronomy, University of Pennsylvania, Philadelphia, PA 19104*

Disordered mechanical systems can deform along a network of pathways that branch and recombine at special configurations called bifurcation points. Multiple pathways are accessible from these bifurcation points; consequently, computer-aided design algorithms have been sought to achieve a specific structure of pathways at bifurcations by rationally designing the geometry and material properties of these systems. Here, we explore an alternative physical training framework in which the topology of folding pathways in a disordered sheet is changed in a desired manner due to changes in crease stiffness induced by prior folding. We study the quality and robustness of such training for different 'learning rules', that is, different quantitative ways in which local strain changes the local folding stiffness. We experimentally demonstrate these ideas using sheets with epoxy-filled creases whose stiffnesses change due to folding before the epoxy sets. Our work shows how specific forms of plasticity in materials enable them to learn non-linear behaviors through their prior deformation history in a robust manner.

Metamaterials [1, 2] and smart materials [3] are often designed to show specific behaviors. For example, mechanical topological insulators localize response to forces [4, 5] while elastic networks with allostery communicate deformations over a long range [6–8]. More complex mechanical structures can show a specific deformation, e.g., a smile-shaped deformation, in response to a spatially textured pattern of forces [9]. Most commonly, mechanical systems are rationally designed to show such behaviors by searching parameter space on a computer [10, 11]. However, an alternate approach explored recently is that of *physical learning* [12–16]: during a period of training, the material is shown examples of the desired behavior, prompting autonomous changes in the material parameters that promote the desired behavior. No computers are involved in optimizing the properties of such a system [17–19].

Physical learning is a more constrained way of exploring parameter space than optimization on a computer. However, an autonomous physical learning process offers the advantage of learning from real examples of stimuli and response [20] (as opposed to a theoretical specification of the problem) and does not rely on an accurate model of the material [21]. Physical learning might also allow for continual learning of new functionalities *in situ*, as requirements change [14]. A major open question is what kinds of local adaptive processes available in real systems constrain physical learning [12]. Recent work has shown that natural processes within an EVA foam network can train the network for an auxetic response by simply aging the material in different configurations [13]. Broader questions remain - what is the impact of different kinds of local learning dynamics on the feasibility and quality of learning?

Here, we explore how the quality of physical learning depends on local adaptive processes (which we call 'learning rules') through theoretical analyses and an experimental demonstration. We focus on training a fundamentally non-linear feature in marginal mechanical systems, a bifurcation point [22–27]. Mechanical bifurca-

tions occur at degenerate configurations from which multiple non-linear zero modes are accessible. Bifurcations cannot be described by a linear approximation even for small deformations since the energy vanishes to two leading orders; they correspond to singularities of the energy function with an excess of linearized zero modes and self-stress states that disappear at next to leading order.

Bifurcation points can potentially be exploited to create multi-functional systems [15] and have been studied in the context of mechanical linkages [28–30] for robotics and topological meta-materials [26]. However, bifurcations can also make the system hard to control [31]. For example, folding outcomes at these singularities can be unpredictable and depend on the precise spatial pattern of forces used [27, 32–34]. While generic mechanical systems show bifurcations in some parts of configuration space [35–37], bifurcations are especially a problem for thin creased sheets because the flat state configuration is necessarily degenerate [27, 32, 38]. In particular, creased thin sheets with nominally 1 degree of freedom (according to Maxwell counting), often called 'self-folding origami', always have a bifurcation at the flat state (henceforth referred to as a "flat state bifurcation") that is the meeting point of an exponentially large number of distinct folding modes. Consequently, such 'self-folding' sheets are hard to control at the flat state (despite the name) since the precise spatial pattern of forces applied will determine the folding geometry.

We focus on the training of such creased thin sheets [39–41] to manipulate the bifurcation point in configuration space (Fig.1A); in particular, we seek to increase the fraction of all force patterns that result in one folding pathway (i.e., attractor size, Fig.1B) through a physical learning rule - crease softening due to folding (Fig.1C, Fig.1D). We find that successful training relies on creating heterogeneity in stiffnesses across the sheet. However, this heterogeneity can rapidly diminish with further training for some classes of learning rules while other classes of learning rules, threshold-like in strain, are more robust. We test some of these ideas with an experimen-

tal prototype in which a sheet with epoxy-filled creases is folded back and forth along one pathway at a bifurcation. Such folding during the 'training period' (i.e., before the epoxy sets) extrudes epoxy to different extents in different creases, creating a heterogeneous system. We test the trained sheet by applying different forces and find successful training in systems with 4 and 7 creases.

RESULTS

Training and Stiffness heterogeneity

We begin with a theoretical study of crease patterns made of 4-valent vertices as shown in Fig.1A. Maxwell constraint counting gives this system 1 degree of freedom but in reality, this structure has two non-linear 1 degree of freedom pathways that meet at a bifurcation at the flat state [42]. As a toy model of energy near a generic bifurcation, consider $E(x, y) = \lambda x^2 y^2$ where x, y parameterize deformations of a mechanical system. Motions along $x = 0$ and $y = 0$ are true zero energy pathways, staying at zero energy for large deformations. However, a linearized analysis at $(x, y) = (0, 0)$ suggests a 2-dimensional vector space of zero modes (along with a self-stress state if we had a mechanistic model); further, any small deformation along $x = 0$ or $y = 0$ will reduce the zero mode space to 1 dimension (and eliminate the self-stress mode). Thus, any linearized analysis will fail to identify the true zero modes $x = 0$ and $y = 0$. On the other hand, any spatial pattern of forces applied to a 4-vertex [27] in its unfolded flat state will result in folding along one of the two zero energy folding pathways.

The non-linear force-response relationship of disordered mechanical systems at such bifurcations can be summarized by an 'attractor diagram', shown schematically in Fig.1B. The space is a 2-d schematic representation of high-dimensional space of spatial force patterns. Each shaded region represents one of the discrete folding outcomes that is realized for all force patterns represented by that region. Earlier work has shown that this attractor structure can be changed by changing the geometry [27, 32], pre-biasing preferred directions [43–45] of the sheet, or controlling the relative stiffness of different creases [46].

Typically, solving the inverse problem for attractors requires a complex computer algorithm; for example, Linear or Quadratic Programming algorithms on a computer [46] can determine crease stiffnesses that eliminate all but a chosen pathway in a saddle-node bifurcation - a local bifurcation in the energy landscape of a dynamical system, where minima collide with adjacent maxima and both disappear as the parameters of the dynamical system is changed (in this case, changing the stiffnesses of the origami creases). After the insertion of these calculated crease stiffnesses, the origami sheet folds only along a chosen desired pathway. Every other folding pathway, hitherto, accessible is now eliminated; as the energy min-
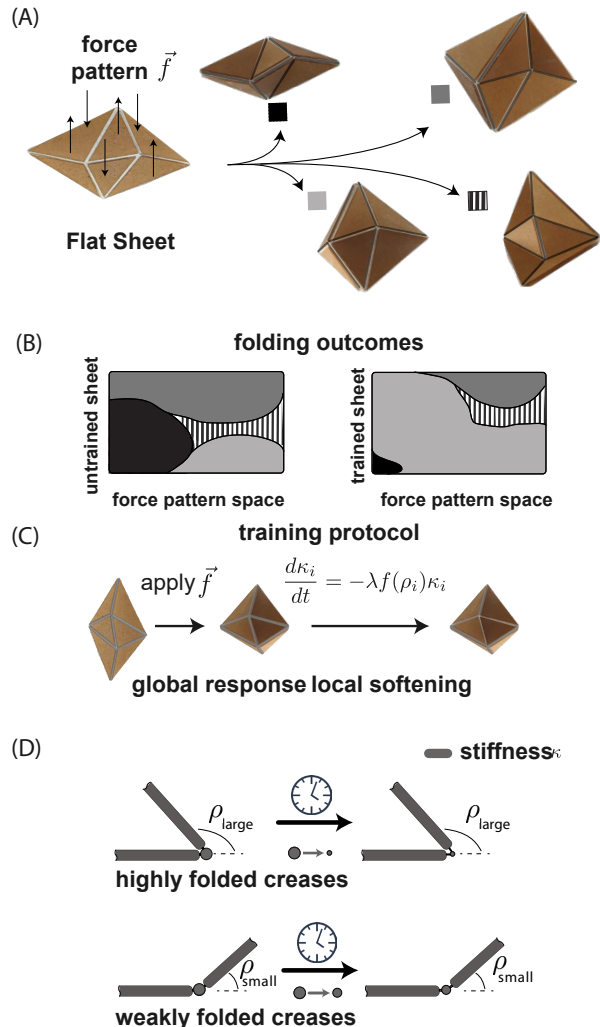

FIG. 1. The topology of folding pathways at a bifurcation can be changed through a physical training protocol. (A) Thin creased sheets can fold along distinct folding pathways that bifurcate from the flat state with outcomes determined by the spatial force pattern. (B) A 2-d schematic representation of high-dimensional attractors in the space of force patterns. Each colored region represents one of the discrete folding outcomes that is realized for all force patterns represented by that region. Specific attractors can be enlarged, shrunk or eliminated by changing crease stiffnesses through design or physical learning. (C,D) We model a physical learning process that changes a crease i's stiffness κ_i (about the flat state) based on its folding strain ρ_i.

ima eliminated correspond to the myriad folded modes accessible from the rest/unfolded state. Here, we investigate whether this same inverse problem can be solved by the sheet itself through a natural physical process, with no computers involved.

Throughout this paper, each crease, i, has a 'crease stiffness', κ_i which refers to the stiffness for the folding strain (or folding angle) about the flat state (i.e., un-

strained/unfolded state) with rest angle maintained at zero; i.e., each crease, i has a folding energy $(1/2)\kappa_i\rho_i^2$ for folding strain ρ_i (see Fig.1D) and crease stiffness κ_i. Thus, this stiffness does not prefer any folding orientation ($\rho \to -\rho$, which is known as mountain-valley symmetry) and only depends on the magnitude of the folding strain/angle of the creases, ρ_i^2. In contrast, a creased sheet of paper develops non-zero rest angles at each crease that breaks the mountain-valley symmetry ($\rho \to -\rho$) at creases and maintains the sheet away from the flat state bifurcation, without actually reshaping the bifurcation itself [46]. In this work, we focus on the non-trivial problem of shaping bifurcations, while maintaining mountain-valley symmetry at each crease, so the trained sheet can still be completely flattened to its unfolded/rest state. Consequently, our trained sheet can symmetrically access either the positive or negative components of a given folding pathway.

As a first pass, we considered learning rules of the type shown in Fig.1C and Fig.1D that softens different creases based on the current folding strain:

$$d\kappa_i/dt = -\lambda\rho_i^2\kappa_i. \qquad (1)$$

where λ, the 'learning rate', sets the learning timescale.

We have chosen to study these crease-softening learning rules because they are the behavior expected of most materials. While there are materials that harden when strained, these require deformations in the plasticity region and far away from the rest state, invalidating the linear-spring folding energy assumption - $(1/2)\kappa_i\rho_i^2$.

As a case study, we begin by applying the above learning rule to 4-vertex shown in Fig.2A; the 4-vertex generically has two distinct folding branches that meet at the flat state bifurcation[42]. We simulated a training process in which the vertex initially has creases of equal stiffness κ_i^0; the sheet is folded repeatedly (using a spatial pattern of forces) along the positive and negative components of one of the two pathways at the bifurcation. The sheet is folded to a configuration of finite strain and the parameters κ_i are updated according to learning rule above for a time interval τ. The sheet is then relaxed back to the flat state and re-folded with the negative of the same pattern of forces and the learning process is continued. See Appendices for parameters. We test the attractor size of each pathway throughout training; the attractor size is determined by applying a library of 500 randomly chosen spatial pattern of folding torques to the creases and counting the fraction of folding torques that result in the chosen folding pathway. We assume that testing does not cause further changes in the stiffnesses κ_i in our simulations (though a real system would continue changing due to testing).

We find that during training, different creases fold to different extents ρ_i in specific ratios characteristic of the branch we fold along. Consequently, the learning rule Eq.1 creates heterogeneity in the initially homogeneous creases stiffness κ_i. When crease stiffnesses are relatively heterogeneous, the attractor size of the chosen pathway
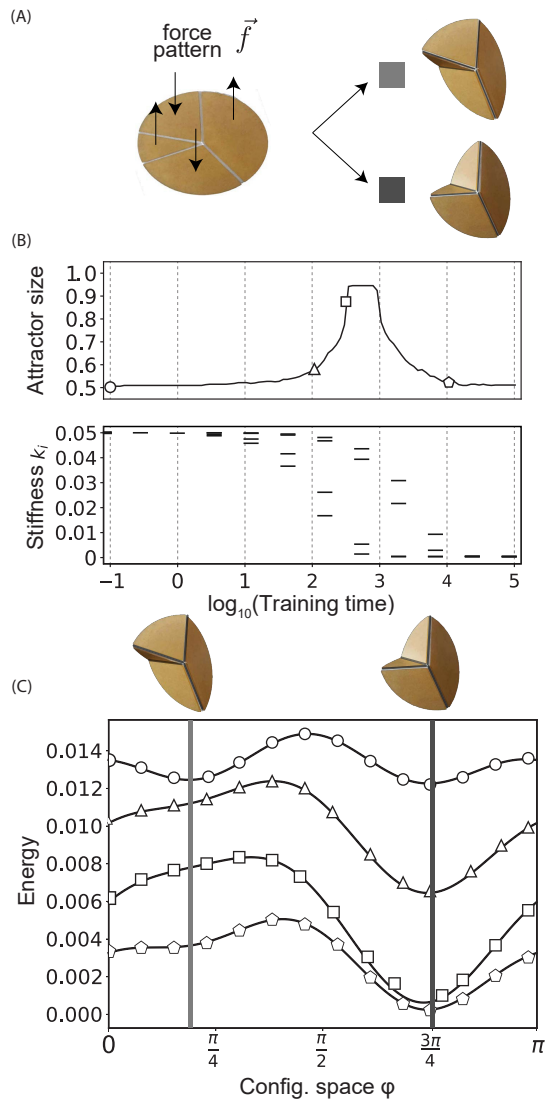

FIG. 2. Eliminating a select folding pathway for a 4-vertex through physical training. (A) A single 4-vertex has two distinct folding modes (light-grey, dark-grey). (B) The dark-grey pathway's attractor size during a training process in which the 4-vertex is folded by a fixed force pattern repeatedly. The stiffness κ_i of each crease, i, are represented by four horizontal lines at each time point during training; all κ_i start at the same stiffness and decrease according to Eq.1. κ_i are in units of the bulk modulus of the stiff faces. Crease stiffnesses, κ_i, become heterogeneous during training, before becoming homogeneous again upon over-training. (C) Energy landscape of a sheet at different points during training (ϕ is an angular coordinate in 2-dimensional null space; see Appendices for details). Landscape before training (circles) and after over-training (pentagons) show two distinct minima; but when attractor size ~ 1 (squares), light-grey's minimum is eliminated via a saddle-node bifurcation. Note in the under-trained regime (triangle), the attractor size is below 1, but well above the initial value of 0.50

increases from an initial value of 0.50 to nearly 1, i.e., nearly all spatial patterns of forces result in the chosen folding pathway; see Fig.2B. However, further training reduces the heterogeneity in creases as all stiffnesses approach zero. In this 'overtrained' regime, the attractor size of the desired pathway drops down to 0.50 again, no bigger than for the initial untrained sheet; see Fig.2B.

To illustrate the phenomenon of saddle-node bifurcation, we computed the energy of the origami sheet in different folded configurations, while its crease stiffnesses, κ_i were evolved by the learning rule, Eq.1. We studied folded configurations within the null space of the origami's potential at the flat state. The origami's potential is defined by three non-linear constraint equations for each vertex. The sum of squares of the residue of these constraint equations for a given folded configuration gives the energy of the origami associated with only the vertex of the origami (energy of crease stiffness is not included). To study folding just away from the flat/unfolded state, we can linearize these three constrain equations around the flat state into a $3 \cdot V \times M$ matrix H, where M is the number of creases in the origami pattern and V is the number of vertices in the origami pattern. However, in the flat state, two of the three constrain equations become degenerate, thus reducing H to a $2 \cdot V \times M$ matrix. The kernel of this $2 \cdot V \times M$, H matrix defines the null space of the origami potential at the flat state. For a single vertex with 4 creases, applying the rank-nullity theorem, we see that the null space is 2-dimensional [46]. We parameterize this null space with the variables r and ϕ. We selected a circle (defined as $r = 0.5$) in this null space and computed the energies of various folded configurations represented by points on the circumference of this circle. Since this is a null space of the origami potential at the flat state, the only non-zero energy component left is the energy resulting from the stiffnesses of the origami creases. An energy minimum in this energy plot (Fig.2C) corresponds to the existence of a stable folded configuration. For untrained sheets, we see two minima corresponding to the two true non-linear folding modes. During training (i.e. the evolution of the crease stiffnesses by the chosen learning rule), the attractor size of one of these true non-linear folding modes is reduced to zero, as the mode is destroyed in a saddle-node bifurcation. This is illustrated in Fig.2C (see light-grey line), as the local minimum on the left gradually transforms to a local maximum in the course of training. In the overtrained regime, the eliminated mode (local minimum on the left) reappears and we find that both pathways are accessible in response to some spatial patterns of forces (See images of the two modes atop Fig.2C).

Hence, we find that training can solve an inverse problem for non-linear behavior, namely that of eliminating one select branch in a saddle-node bifurcation and, thus, changing the topology of pathways. Further, successful training is correlated with the development of stiffness heterogeneity (see Fig.2B); this observation is an example of a larger principle that disordered systems can learn

because the information must be stored in the trained degrees of freedom; homogeneous creases cannot store such information. Finally, we find that this particular training rule is prone to over-training and homogenization of creases if training is carried on for too long (see Fig.2B).

We have found that heterogeneity in the crease stiffnesses stores the learned information about the desired pathway; but the learning rule that created the desired heterogeneity also erases that information upon further training. Similar erasure of trained response was observed in systems like cyclically sheared Brownian suspensions and charge-density wave conductors [47].

Robustness of different learning rules

Qualitatively, many real materials soften with strain as captured by the learning rule Eq.1, but might differ quantitatively. Different materials will have different learning rules; some might soften proportionally to their strain or to higher powers of their strain and yet others might be even more sensitive, softening only for strains above a specific threshold. Other non-equilibrium systems can show more complex learning, where synaptic weights or learning degrees of freedom can both strengthen or soften over time; we do not investigate those cases.

We investigated whether such quantitative differences in material properties might have a qualitative effect on the quality and robustness of learning. We considered families of rules of the type:

$$d\kappa_i/dt = -\lambda f(\rho_i)\kappa_i. \tag{2}$$

The first family we considered were different polynomial forms $f(\rho_i) \sim \rho_i^N$. Note that Eq.1 is the case where N=2 (See Fig.3A). The second family, defined by a Hill coefficient M, $f(\rho_i) \sim \rho_i^M/(\rho_i^M + T^M)$ corresponds to sigmoidal dependence often seen in real systems; small strains do not cause significant aging or change in stiffness but strains above a characteristic threshold T cause stiffness changes; further the precise amount of strain does not matter beyond this threshold T (See Fig.3A).

We trained a larger disordered creased sheet with 13 creases and 4 vertices (See Fig.3B); this sheet had 16 non-linear modes meeting at the flat state bifurcation. We used the same training protocol as for the single vertex (4-vertex) in Fig.2: we selected one pathway as the desired pathway and applied the learning rule as the structure was folded repeatedly into the positive and negative components of the selected pathway. As earlier, we quantified successful learning by the attractor size of the desired pathway, i.e., folding the sheet with a library of 500 random force patterns and computing the fraction of force patterns that result in a specific folded mode. We assume that stiffnesses do not change during such testing.

Among polynomial learning rules $f(\rho_i) \sim \rho_i^N$, we found that training rules with higher order polynomials (higher N) resulted in better training in large
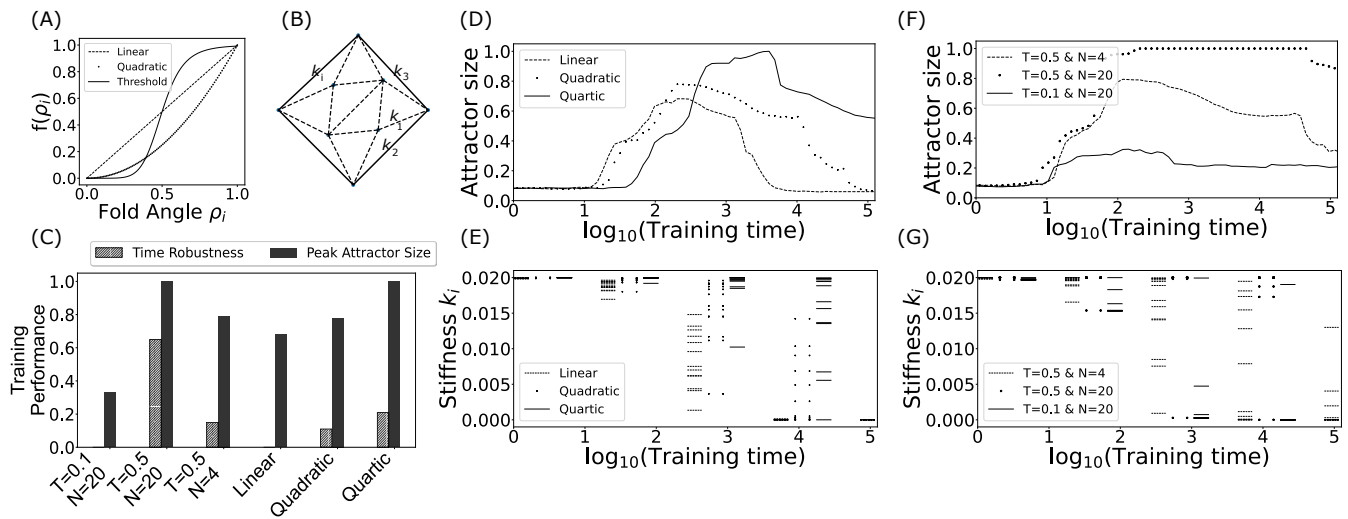
FIG. 3. Quality and robustness of learning depend on the learning rule. (A,B) For the sheet with 13 creases shown, we model a family of 'training rules' with crease stiffness κ_i that change with strain ρ_i (which has been normalized and, thus,ranges from 0 to 1) in a polynomial $f(\rho_i) \sim \rho_i^N$ or threshold $f(\rho_i) \sim \rho_i^M/(\rho_i^M + T^M)$ manner. (C) Learning quality (peak attractor size; see D,F) and robustness (length of training time over which attractor size > 0.70; see D,F) for different learning rules are explored here. (D) With $f(\rho_i) \sim \rho_i^N$ rules, the attractor size of the desired pathway rises to a peak before falling. The peak attractor size (quality of learning) increases with N. (E) The stiffness of each of the 13 creases, i, of the origami are represented by the 13 horizontal lines. They all start out with the same stiffness and decrease according to the different polynomial learning rules indicated by the markers of the line. κ_i are in units of the bulk modulus of the stiff faces. The polynomial rules also show a regime of over-training where stiffness κ_i become homogeneous again as all κ_i go to zero. The horizontal lines representing the crease stiffnesses for the different polynomial learning rules are plotted at select times, so as to avoid the lines of the different polynomial learning rules from overlapping. (F) Attractor size vs training time for threshold learning rules. (G) The stiffness of each of the 13 creases, i, of the origami are represented by the 13 horizontal lines. They all start out with the same stiffness and decrease according to the different threshold learning rules indicated by the markers of the line. κ_i are in units of the bulk modulus of the stiff faces. Crease heterogeneity grows with training, and does not decrease (no overtraining) with continued training for some of the threshold learning rules (asterisked line).The horizontal lines representing the crease stiffnesses for the different threshold learning rules are plotted at select times, so as to avoid the lines of the different threshold learning rules from overlapping.

origami patterns. We found a higher attractor amplitude (i.e. peak attractor size) and a greater training time robustness - learning quality stayed higher for longer (See Fig.3C). However, all polynomial learning rules were still susceptible to overtraining, during which the crease stiffness heterogeneity was lost (See Fig.3D, Fig.3E). With threshold-like learning rules, the over-training problem was nearly eliminated (See Fig.3F). We found that creases that fold less than the threshold T do not soften at all and hence the learned heterogeneity in stiffness is maintained over time. However, there is a trade-off; the threshold T of the learning rule needs to be within the range of strains experienced during training. If T is too large, no training would occur. If T is too small, training will fail to create sufficient heterogeneity in stiffnesses κ_i to encode information about the desired mode (See Fig.3G).

Moreover, the heterogeneity of crease stiffnesses arrived via threshold learning protocol (where some creases are untrained while others are trained during the training protocol, resulting in creases with stiffnesses and others without stiffnesses), suggests the concept of "critical creases", i.e. a desired folding pathway can be defined by a specific set of creases having stiffnesses and others without stiffnesses; a binomial kind of distribution (1s and 0s).

Experimental demonstration

With these theoretical results in place, we demonstrated these ideas with an experimental prototype. While many previous works have implemented creased sheets in systems ranging from graphene on the nanoscale [48] to mylar and cardboard on the mesoscale [49] to solar panels on satellites [50], these works generally have fixed stiffness in different creases and thus an inability to learn folding behaviors. We note that paper or cardboard is affected by folding but typically develops a non-zero rest angle upon folding and is thus likely to fold in the same way again. But as noted earlier, such a displacement from the bifurcation does not reshape the bifurcation which still exists if the sheet is forced into the flat state. Here, we create a prototype

that maintains $\rho \to -\rho$ symmetry at each crease and hence can still be laid flat after training.

We created a sheet with gullies at creases by sandwiching a Tyvek sheet between acrylic pieces that were laser cut to serve as stiff faces of a crease pattern. See Fig.4A. Consequently, the creases correspond to gullies of width w (set by the gap between adjacent acrylic pieces) and depth h (set by the thickness of acrylic) on both sides of the sheet. A slow setting epoxy solution is created from a mixture of epoxy resin and a curing agent in the ratio $1:2$. The creases are filled with epoxy on both sides of the sheet; the epoxy takes ~ 60 minutes to set. See Appendices for details. During this setting time (the 'training phase'), the crease is manually folded to an angle $+\rho$, flattened to the rest state (i.e. when all crease fold angles $= 0$) and then folded to angle $-\rho$ in the other direction. Such folding will extrude an amount of epoxy $h(|\rho_i|)$ from the crease gully that depends on the magnitude of folding $|\rho_i|$. Only epoxy remaining inside the crease determines the stiffness of that crease at the end of the training phase. Thus, the amount of epoxy extruded $h(|\rho_i|)$ determines the change in stiffness $\Delta\kappa$ during training and thus determines the form of the learning rule in Eq.2. By folding in both directions $(\pm\rho)$ during training, we maintain mountain-valley symmetry and zero rest angles at the crease in its flat/rest state; consequently, the trained sheet can still be laid flat. The training protocol is illustrated in Fig.4B.

We constructed a vertex with 4 creases (studied theoretically in Fig.1), resulting in two folding modes (light-grey and dark-grey) shown in Fig.4C. Initially, before any epoxy is added, all creases are free folding. We tested the response of this free folding vertex to forces applied at different points along the boundary of one of the sectors. We found that forces at 3 of 7 locations leads to the dark-grey folding mode while forces at the 4 locations result in the light-grey folding mode (See Fig.4C). Forces applied to all points in the other sectors led to either the dark-grey or the light-grey mode. We then filled the creases with slow setting epoxy, marking the start of the training phase. We manually folded the vertex into a selected mode (dark-grey mode) with characteristic folding angles $\rho_i^{darkgrey}$ at each crease, reverted to the flat state and folded along the negative component $-\rho_i^{darkgrey}$ of the same dark-grey pathway. We folded until the largest folded crease could not be folded further; in this way, the magnitude of folding is approximately the same along the positive and negative components of the pathway and over multiple instances of folding during training. Throughout this training, the vertex was clamped in a vertical configuration but was rotated periodically to prevent epoxy from flowing out of the creases due to gravity. We repeated this folding process for 60 minutes, folding back and forth along the positive and negative components of the dark-grey mode. See Appendices for details of the experiment.

After the epoxy set, we found that forces at all 7 test locations now lead to the dark-grey mode as illustrated in
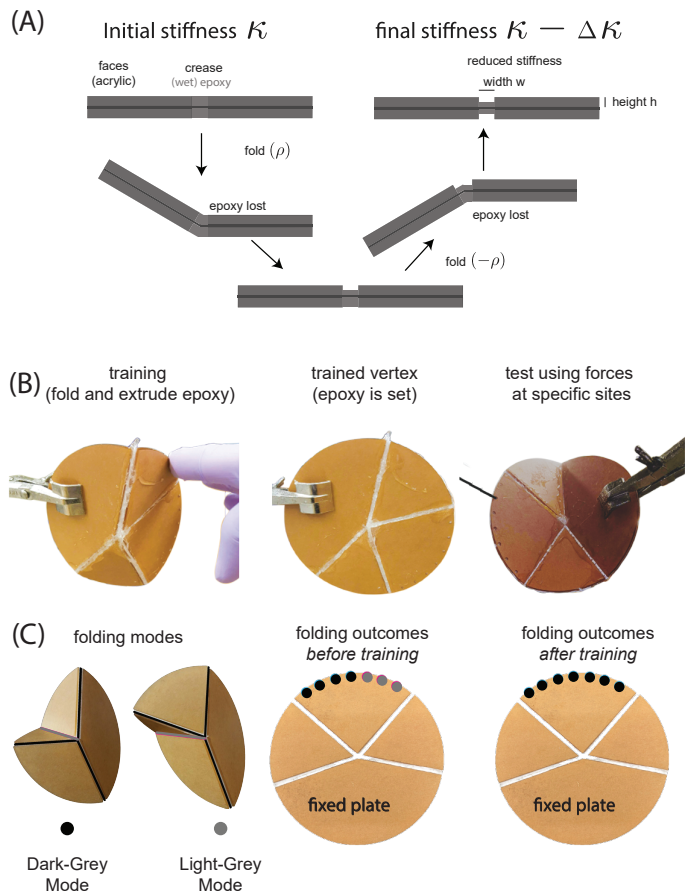

FIG. 4. Experimental realization of training through epoxy extrusion. (A) (schematic) We created creased sheets by sandwiching a thin membrane between thick acrylic sheets that serve as stiff faces; the resulting creases of width w and height h are filled with epoxy (black lines on creases). Folding by angles ρ_i before the epoxy sets (the training period) will extrude epoxy; creases with larger ρ_i will extrude more epoxy, resulting in lower stiffness κ after the epoxy sets. (B) A 4-crease vertex with epoxy filled creases was trained by repeatedly folding along one of the two pathways during the setting period; folding is repeated along positive and negative components of the chosen pathway to avoid any directional folding bias in the creases. (C) Testing: Folding outcomes are determined for folding forces applied at different locations. The untrained sheet folds along two distinct pathways depending on location of applied force (light-grey and dark-grey dots). The trained sheet folds along only one pathway for all folding forces (dark-grey dots), demonstrating an increased attractor for the dark-grey pathway.

Fig.4C, showing that the training procedure had modified the flat state bifurcation, presumably by eliminating the light-grey branch at a saddle-node bifurcation away from the flat state [46]. Using a fresh sample, we also successfully repeated the training process above to retain the light-grey mode and eliminate the dark-grey mode instead.

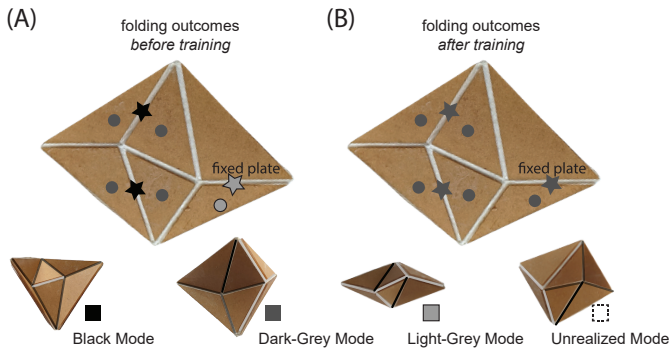To see if the principles behind this simple demonstra-

FIG. 5. Learning to expand a select attractor in a complex sheet. A sheet with 7 creases and 2 vertices has 4 distinct folding pathways (shown at the bottom). (A) Before training, three pathways are accessible by forces applied to different locations shown (circles) or by torques applied to specific creases (stars). (B) The creases were filled with epoxy and folded back and forth along the dark-grey pathway as the epoxy set (the training period). After training, the sheet was 'tested' with the same forces and torques used in (A). All test forces and torques now result in the dark-grey pathway, indicating an expanded attractor size for that pathway.

tion are robust enough to work in more complex disordered systems, we attempted training on a sheet with 7 creases, 2 vertices and thus 4 distinct pathways at the bifurcation; see Fig.1A. As shown in Fig.5A, the untrained sheet folds along 3 of those 4 pathways for test forces applied to the center of different faces with one face held clamped. (The fourth pathway requires torques at specific creases that cannot be realized by forces at a single face in the clamped configuration we used.) We filled the creases with epoxy and trained with the same protocol as earlier, manually folding along a select pathway (the dark-grey pathway), flattening the sheet, folding along the negative branch of that pathway and repeating the process for 60 minutes. After the training process is completed and the epoxy has set, we tested the sheet with the same test forces applied to the faces when it was untrained; we now find that all forces lead to folding along the target dark-grey pathway as illustrated in Fig.5B. Thus, the flat state bifurcation has been successfully trained to eliminate the other pathways, presumably through saddle-node bifurcations away from the flat state.

DISCUSSION

The study of bifurcations in mechanical systems has attracted attention from mathematicians [51], roboticists [52, 53] and physicists [27, 32, 46]. Most work has focused on changing the structure of bifurcations by rationally changing parameters such as lengths of the elements. Our work here shows at least some versions of this design problem can be solved by changing stiffness of joints through a physical training protocol. Our

work further suggests that bifurcations might be physically trainable in mechanical linkages where the lengths of elements change according to learning rules; changes in length have been used as a basis for physical training in other contexts [13, 16, 54, 55].

The experimental demonstration here illustrates how a generic physical process - the extrusion of material at creases - can naturally implement 'learning rules' that confer specific functionality on the system. Other materials naturally show softening with strain [13], possibly allowing for the implementation of different functional forms of our learning rules.

The locality of physical learning in mechanical systems contrasts the global nature of most machine learning algorithm, where learning parameters are non-locally updated (gradient descent protocols). The training rules are local, softening each crease in response to strain in that crease. Further, even at the end of training, the learned stiffness in any one crease does not immediately favor one folding pathway over another. However, creases that meet at a vertex [49] have non-linear interactions that constrain their relative folding; such interacting creases are able to collectively learn and encode information about a desired pathway even if each individual crease does not select a pathway by itself.

While we trained for one attractor to grow and occupy most of the force pattern space, one can also train a system for multiple attractors [15]. Such training can create a mechanical pattern recognizer, folding into one configuration in response to one set of force patterns and a distinct configuration in response to a different set of force patterns. Unlike similar responsive materials designed on a computer, the learning paradigm here lets structures learn *in situ* from real examples of force patterns [13].

I. APPENDICES

A. Theory

Theoretical Modeling of Self-Folding Sheets

We model creased sheets using energy-based models developed in previous work [39, 49, 56]. We assume that creases have a stiffness modeled by torsional spring elements on each crease [15, 27, 46]. We briefly review the elements of this model as we build upon this work to simulate the physical learning of desired folding pathways of self folding origami sheets.

The energy of thin sheet origami is dominated by face bending governed by mechanical constraints at the origami vertices. Each vertex contributes 3 constraints on the folding angles of creases around it [56]. Take a vertex surrounded by N creases denoted with an index i and each folded to an angle ρ_i. At the flat state, all $\rho_i = 0$, which trivially satisfies all mechanical constraints. One can write down an expansion for these 3 non-linear constraints $T_a(\rho_i)$ [27]. The energy of the folded origami is taken as the sum of squares of the residues of these constraints $E_{\text{Vertex}} \sim \sum_a T_a^2$, which is independently summed over different vertices [46]. The energy due to the stiffness in the creases is $E_{\text{Crease},i} = \frac{1}{2}\kappa_i \rho_i^2$ as discussed in the main text. Thus, the total energy of a folded sheet is the sum of vertex and stiff crease energies

$$E_{\text{sheet}}(\rho_i) = \sum_{v \in vertices} \sum_{a=1}^{3} T_{va}^2 + \frac{1}{2} \sum_{i \in \text{creases}} \kappa_i \rho_i^2. \quad (3)$$

In the learning protocol presented in this work, the crease geometry is fixed and so are the vertex constraints T_{va}. The change in the energy of a folded configuration ρ_i during training stems directly from the change in the individual crease stiffness values

$$\frac{dE}{dt} = \frac{\partial E}{\partial \kappa_i}\frac{d\kappa_i}{dt} = \frac{1}{2}\rho_i^2 \frac{d\kappa_i}{dt}. \quad (4)$$

Simulated Sheet Folding

Using the energy model described previously, we simulated the folding of the self folding origami via several numerical folding methods [46].

Origami sheets are numerically folded similarly to the way described in [15]. The folded sheet's configurations are initialized at

$$\rho_{i0} = \rho \frac{\tau_i}{||\tau_i||}$$

by a set of external folding torques (τ_i) on the creases with $\rho \equiv ||\rho_i||$, the folding magnitude, chosen to be $\rho = 0.5$. However, this initialization point is typically not an

energy minimum on the surface of the hyper-sphere of radius ρ. Thus, we numerically relax the sheet to a local minimum of Eq.3 using MATLAB, subject to a constraint that fixes the folding magnitude ρ:

$$\begin{aligned} \underset{\rho_i}{\text{minimize}} \quad & E_{\text{sheet}}(\rho_i) \\ \text{subject to} \quad & ||\rho_i|| = \rho. \end{aligned} \quad (5)$$

This protocol mimics the experimental fast folding of origami sheets, and the clamping of one crease at a specific folded dihedral angle. It was tested and validated in [46]. The results of this folding protocol are similar to torque based folding of sheets using Newtonian methods.

Simulation of Sculpting Folding Pathways Through Physical Learning

Starting with Eq.4 above we see that the evolution of the energy landscape and, thus, folding pathway is driven by $\frac{d\kappa_i}{dt}$. Physical learning is introduced by the dynamic specification of $\frac{d\kappa_i}{dt}$ defined by various physical learning rules, which are functions of the fold angles of the mode $\rho_i^{Teacher}$, whose attractor size we desire to expand:

$$d\kappa_i/dt = -\lambda f(|\rho_i^{Teacher}|)\kappa_i. \quad (6)$$

where λ, the 'learning rate', sets the learning timescale and $\rho_i^{Teacher}$ is a vector defining the fold angles of the creases of the desired mode whose attractor size we want to increase. Note that $\rho_i^{Teacher}$ is obtained by folding the creases of the origami with an external torque, $F_i^{Teacher}$ as described above. We generated the components of $F_i^{Teacher}$ by first randomly selecting a number from a normal distribution. Next we normalized this vector and used it to fold the creases of the origami as described above. We checked if the scalar product between the normalized vector and the resulting normalized folded mode is greater than 0.99. If it is not, we generate another $F_i^{Teacher}$ by selecting another random set of numbers for its components and check if the new vector and its resulting folded mode have a scalar product greater than 0.99. If the scalar product is greater than 0.99, then the final resulting folded mode is then normalized and assigned to $F_i^{Teacher}$. The learning rule is specified by $f(\rho_i^{Teacher})$ which can be a linear, quadratic or a threshold function of $\rho_i^{Teacher}$. We simulated a physical learning process in which the creases initially had a uniform stiffness $\kappa_i^0 = 0.05$ (for single-vertex origami) and $\kappa_i^0 = 0.02$ (for double vertex origami). A unit of stiffness represents the bending modulus of the stiff faces of the origami. The crease stiffnesses are evolved with a learning rate $\lambda = 0.01$ per training round. Thus, we have specified not just a teacher for the physical learning process, $F_i^{Teacher}$, but also a curriculum or learning rule, $f(\rho_i^{Teacher})$, for the physical learning process.

Simulation of Testing Protocol

After each round of training via physical learning as described above, the attractor size of the desired mode is computed. To calculate the attractor size, a set of an array of test torques, $TestTorqueSet$ is created. Each element of the set, $TestTorqueSet$ is defined by a vector $F_i^{external}$, whose components, $F_{i,j}^{external}$, represent the magnitude of the torque applied to each crease. Each vector $F_i^{external}$ is normalized and used to fold the creases of the self folding origami sheet as described above. Folding with each external torque, $F_i^{External}$, results in a folded mode ρ_i^{Folded}. Note that the folded mode vector, ρ_i^{Folded} is also normalized as well. This folded mode, ρ_i^{Folded} is compared to the desired mode, $\rho_i^{Teacher}$ whose attractor size we seek to increase.

To compare the folded mode, ρ_i^{Folded}, with the desired mode, $\rho_i^{Teacher}$, we take the scalar product between both vectors. If the scalar product between the two vectors is above 0.9, then we consider the two modes as similar, and one and the same. We count the number of external torques, $F_i^{External}$, in the set $TestTorqueSet$, whose folded mode, ρ_i^{Folded}, are considered similar to $\rho_i^{Teacher}$. We then express this count number as a fraction of the cardinality of the set $TestTorqueSet$. This fraction defines the attractor size of the desired mode.

Quality of Learning

Two agents drive the physical learning process: the teacher, $F_i^{Teacher}$, and the curriculum/learning rule, $f(\rho_i^{Teacher})$. We found the kind of teacher selected does not affect the quality of the physical learning as long as it results in the desired folded mode. Hence, the quality of learning is determined by the kind of learning rule selected. We quantify the quality of learning for various learning rules with two parameters: the peak attractor size attainable and the time robustness of the learning rule. The peak attractor size compares the maximum attractor size achieved for a desired mode for the different learning rules. Meanwhile, the time robustness measures the percentage of the training round for which the self folding origami is optimally trained (i.e. attractor size is above 0.70). The time robustness is a measure of the training protocol's resilience against over-training.

Calculation of Energy Landscape for A Single Vertex (4-vertex) Origami

To illustrate the mechanism by which physical learning alters the energy landscape of the self folding origami via a saddle-node bifurcation, we plotted the energy, Eq.3 of the different folded configurations at several points during the training of the origami. After each round of training, the stiffnesses in the creases of the single vertex (4-vertex) changes and the energy landscape of

the folded configuration space is re-computed. This time-energy landscape plot shows the elimination of the unwanted folding pathway (mode) via a saddle-node bifurcation, and the preservation of the desired folding pathway (mode) after several rounds of training. Further training results in a recovery of the previously eliminated mode.

B. Experiments

Acrylic sheet setup

To create a system naturally capable of learning, we exploited an origami system with fresh epoxy totally filled into the crease pattern of the origami. This epoxy is extruded from the creases during the folding of the origami during the training protocol. This results in a final stiffness (after the epoxy sets) that depends on the amount of folding of each of the creases. We laser cut origami patterns in acrylic sheets of thickness 1.5mm; crease lines were designed to have a gap (or width) of 30mm. Test holes of 10mm diameter are laser cut on the acrylic sheet at various strategic positions (along the circumference of the $90°$ plate for the single vertex (4-vertex) and on the center of each plate of the double vertex). Two copies of such acrylic patterns were each glued to both sides of a sheet of Tyvek. The corresponding plates of the origami patterns on each side of the sheet of Tyvek are lined up with each other before the glue sets. After the glue is set, holes for applying testing forces on the faces of the origami plates are perforated. The resulting setup has stiff faces (bending stiffness set by acrylic) and soft creases (stiffness set by the Tyvek sheet). Origami patterns studied were for a single vertex (4-vertex) and double vertex. The single vertex (4-vertex) has four creases radiating from a single vertex at the center of the pattern. The creases of this single vertex (4-vertex) pattern form sector-angles $150°$, $60°$, $90°$, and $60°$. The double vertex pattern with a total of 7 creases consists of two internal vertices; one vertex has the following sector angles $107°$, $123°$, $82°$, and $48°$, while the second vertex is surrounded by sector angles $82°$, $54°$, $99°$, and $125°$. The two vertices are connected by a common crease. This connecting crease serves as the boundary dividing the $82°$ sector plate from the $48°$ sector plate of the first vertex, and the $82°$ sector plate from the $54°$ sector plate of the second vertex. The sector angles, crease lengths, and position of the vertices for both the single vertex and double vertex are specified in a supplementary PDF file which can be used to laser cut these patterns [57, 58].

Epoxy and training

a. Epoxy Mixture An epoxy solution is made by mixing epoxy resin with its curing agent in the ratio 1:2. This mixture is stirred for about five minutes and poured

into the creases of the origami pattern on both sides of the assembly. Note, that if the epoxy had been mixed in the ratio 1:1, upon curing, it would be so stiff that the origami assembly would be difficult to fold, without destroying the assembly; such epoxy when hardened is also brittle and would fracture under a bending moment attempting to fold the origami assembly. Hence, we mix epoxy resin and curing agent in the ratio 1:2, allowing for crease folding upon curing of the epoxy mixture, without disintegration of the origami assembly.

b. Folding of Origami Assembly The origami assembly filled with watery epoxy in its creases is manually folded into the desired configuration that is to be trained for. The origami assembly is trained by manually folding the assembly back and forth along the positive and negative components of a desired folding pathway. This cyclic manual folding between both pairs of the desired mode is repeated for an hour, during which the epoxy solution begins to cure and is no longer watery. A simple folding protocol is utilized to fold the origami assembly into the desired configuration: one of the plates of the origami assembly is fixed while pushing or pulling on any of the other plates of the origami assembly with a normal force or a turning torque exerted at a single contact point on any of the non-fixed origami plates.

c. Training Under Gravity Since the epoxy is still watery during origami training, it needs to be trained on a rotating platform to avoid epoxy from flowing out of the creases due to the influence of gravity. The rotating platform consists of two standing laboratory clamps screwed to the optical table and situated 600mm apart. A rod is horizontally supported by the claws of the two standing laboratory clamps, but the rod is allowed to freely rotate within the claws of the clamp. A lab clamp retort is then fixed clamped (allows for no rotation or slipping) to the rotation-free horizontally placed rod with the claws on one end of lab clamp retort, while the claws on the other end of the lab clamp retort is clamped to one of the plates of the origami (the plate fixed during training as previously described). As one hand is used to exert a normal force or turning torque on one of the free plates of the origami assembly in order to fold it into the positive and negative components of the desired mode, the other hand is used to manually turn the rotation-free horizontal rod. This combined process results in the folding of the origami assembly, while under rotation, and, thus, prevents the flow of the epoxy solution from the origami's creases during this training; while under the influence of gravity.

Emergence of Crease Stiffness

After training the origami assembly, the origami samples are allowed to further cure and are left hanging in the lab for a week. This allows the epoxy solution in the creases to harden, thus, producing an effective stiffness on the creases of the origami.

Testing protocol

The plate of the origami assembly fixed during training is clamped. A 100mm long thread knotted on one end is passed through each of the testing holes of the origami assembly. The threads are gently pulled normal to the surface of the origami plate. Upon pulling each thread in each hole, the origami folds into a given configuration. The resulting configuration for each pull is recorded. The attractor size of the different folding modes of the origami assembly is computed. This process is repeated for both the trained and untrained samples of the origami assembly. The attractor size of the chosen trained mode before and after training are compared to one another.

---

[1] Yongmin Liu and Xiang Zhang. Metamaterials: a new frontier of science and technology. *Chemical Society Reviews*, 40(5):2494–2507, 2011.

[2] Pedro M Reis, Heinrich M Jaeger, and Martin van Hecke. Designer matter: A perspective. *Extreme Mech. Lett.*, 5:25–29, 2015.

[3] Mukesh V Gandhi and BD Thompson. *Smart materials and structures.* Springer Science & Business Media, 1992.

[4] Katia Bertoldi, Vincenzo Vitelli, Johan Christensen, and Martin Van Hecke. Flexible mechanical metamaterials. *Nature Reviews Materials*, 2(11):1–11, 2017.

[5] Adrien Saremi and Zeb Rocklin. Topological elasticity of flexible structures. *Physical Review X*, 10(1):011052, 2020.

[6] Jason W Rocks, Nidhi Pashine, Irmgard Bischofberger, Carl P Goodrich, Andrea J Liu, and Sidney R Nagel. Designing allostery-inspired response in mechanical networks. *Proceedings of the National Academy of Sciences*, 114(10):2520–2525, 2017.

[7] Tsvi Tlusty, Albert Libchaber, and Jean-Pierre Eckmann. Physical model of the genotype-to-phenotype map of proteins. *Physical Review X*, 7(2):021037, 2017.

[8] Le Yan, Riccardo Ravasio, Carolina Brito, and Matthieu Wyart. Architecture and coevolution of allosteric materials. *Proceedings of the National Academy of Sciences*, 114(10):2526–2531, 2017.

[9] Corentin Coulais, Eial Teomy, Koen De Reus, Yair Shokef, and Martin Van Hecke. Combinatorial design of textured mechanical metamaterials. *Nature*, 535(7613):529–532, 2016.

[10] Kenneth Diest. *Numerical methods for metamaterial design*, volume 127. Springer, 2013.

[11] Nicholas E Jackson, Michael A Webb, and Juan J de Pablo. Recent advances in machine learning towards multiscale soft materials design. *Current Opinion in Chemical Engineering*, 23:106–114, 2019.

[12] Nidhi Pashine. Local rules for fabricating allosteric networks. *Physical Review Materials*, 5(6):065607, 2021.

[13] Nidhi Pashine, Daniel Hexner, Andrea J Liu, and Sidney R Nagel. Directed aging, memory, and nature's greed. *Science Advances*, 5(12):eaax4215, 2019.

[14] Menachem Stern, Matthew B Pinson, and Arvind Murugan. Continual learning of multiple memories in mechanical networks. *Physical Review X*, 10(3):031044, 2020.

[15] Menachem Stern, Chukwunonso Arinze, Leron Perez, Stephanie E. Palmer, and Arvind Murugan. Supervised learning through physical changes in a mechanical system. *Proceedings of the National Academy of Sciences*, 117(26):14843–14850, 2020.

[16] Menachem Stern, Daniel Hexner, Jason W Rocks, and Andrea J Liu. Supervised learning in physical networks: From machine learning to learning machines. *Physical Review X*, 11(2):021045, 2021.

[17] Sam Dillavou, Menachem Stern, Andrea J Liu, and Douglas J Durian. Demonstration of decentralized, physics-driven learning. *arXiv preprint arXiv:2108.00275*, 2021.

[18] JF Wycoff, S Dillavou, M Stern, AJ Liu, and DJ Durian. Desynchronous learning in a physics-driven learning network. *The Journal of Chemical Physics*, 156(14):144903, 2022.

[19] Menachem Stern, Sam Dillavou, Marc Z. Miskin, Douglas J. Durian, and Andrea J. Liu. Physical learning beyond the quasistatic limit. *Phys. Rev. Research*, 4:L022037, May 2022.

[20] Menachem Stern and Arvind Murugan. Learning without neurons in physical systems. *arXiv preprint arXiv:2206.05831*, 2022.

[21] Logan G Wright, Tatsuhiro Onodera, Martin M Stein, Tianyu Wang, Darren T Schachter, Zoey Hu, and Peter L McMahon. Deep physical neural networks trained with backpropagation. *Nature*, 601(7894):549–555, 2022.

[22] Jon Kieffer. Differential analysis of bifurcations and isolated singularities for robots and mechanisms. *IEEE T. Robotic. Autom.*, 10(1):1–10, 1994.

[23] P Kumar and S Pellegrino. Computation of kinematic paths and bifurcation points. *International Journal of Solids and Structures*, 37(46-47):7003–7027, 2000.

[24] Yan Chen and Woon Huei Chai. Bifurcation of a special line and plane symmetric bricard linkage. *Mech. Mach. Theory*, 46(4):515–533, 2011.

[25] Davide Bigoni. *Nonlinear solid mechanics: bifurcation theory and material instability*. Cambridge University Press, 2012.

[26] Bryan Gin-ge Chen, Nitin Upadhyaya, and Vincenzo Vitelli. Nonlinear conduction via solitons in a topological mechanical insulator. *Proc. Natl. Acad. Sci. U. S. A.*, 111(36):13004–13009, 2014.

[27] Menachem Stern, Matthew B. Pinson, and Arvind Murugan. The complexity of folding self-folding origami. *Phys. Rev. X*, 7:041070, Dec 2017.

[28] David H Myszka, Andrew P Murray, and Charles W Wampler. Computing the branches, singularity trace, and critical points of single Degree-of-Freedom, Closed-Loop linkages. *J. Mech. Robot.*, 6(1):011006, February 2014.

[29] Lin Li, David H Myszka, Andrew P Murray, and Charles W Wampler. Using the singularity trace to understand linkage motion characteristics. In *ASME 2013 International Design Engineering Technical Conferences and Computers and Information in Engineering Confer-*

ence, pages V06AT07A063–V06AT07A063. Design Engineering Division, August 2013.

[30] D Rocklin, Vincenzo Vitelli, and Xiaoming Mao. Folding mechanisms at finite temperature. *Preprint at http://arXiv.org/abs/1802.02704*, 2018.

[31] Harry G Kwatny, Bor-Chin Chang, and Shiu-Ping Wang. Static bifurcation in mechanical control systems. In *Bifurcation Control*, pages 67–81. Springer, 2003.

[32] Bryan Gin-ge Chen and Christian D Santangelo. Branches of triangulated origami near the unfolded state. *Phys. Rev. X*, 8(1):011034, 2018.

[33] A Gillman, K Fuchi, and PR Buskohl. Truss-based nonlinear mechanical analysis for origami structures exhibiting bifurcation and limit point instabilities. *International Journal of Solids and Structures*, 147:80–93, 2018.

[34] ME Lee-Trimble, Ji-Hwan Kang, Ryan C Hayward, and Christian D Santangelo. Robust folding of elastic origami. *arXiv preprint arXiv:2109.10989*, 2021.

[35] Charles W Wampler. Manipulator inverse kinematic solutions based on vector formulations and damped least-squares methods. *IEEE T. Syst. Man Cyb.*, 16(1):93–101, 1986.

[36] Charles W Wampler, Jonathan D Hauenstein, and Andrew J Sommese. Mechanism mobility and a local dimension test. *Mechanism and machine theory*, 46(9):1193–1206, 2011.

[37] David H Myszka, Andrew P Murray, and Charles W Wampler. Mechanism branches, turning curves, and critical points. *ASME 2012 International Design Engineering Technical Conferences and Computers and Information in Engineering Conference*, pages 1513–1525, January 2012.

[38] Dor Shohat, Daniel Hexner, and Yoav Lahini. Memory from coupled instabilities in unfolded crumpled sheets. *Proceedings of the National Academy of Sciences*, 119(28):e2200028119, 2022.

[39] Thomas C Hull et al. Modelling the folding of paper into three dimensions using affine transformations. *Linear Algebra and its applications*, 348(1-3):273–282, 2002.

[40] Tomohiro Tachi. Generalization of rigid-foldable quadrilateral-mesh origami. *Journal of the International Association for Shell and Spatial Structures*, 50(3):173–179, 2009.

[41] Levi H Dudte, Etienne Vouga, Tomohiro Tachi, and Lakshminarayanan Mahadevan. Programming curvature using origami tessellations. *Nature materials*, 15(5):583–588, 2016.

[42] Scott Waitukaitis, Rémi Menaut, Bryan Gin-ge Chen, and Martin Van Hecke. Origami multistability: From single vertices to metasheets. *Physical review letters*, 114(5):055503, 2015.

[43] Tomohiro Tachi and Thomas C Hull. Self-foldability of rigid origami. *Journal of Mechanisms and Robotics*, 9(2):021008, 2017.

[44] Ji-Hwan Kang, Hyunki Kim, Christian D Santangelo, and Ryan C Hayward. Enabling robust self-folding origami by pre-biasing vertex buckling direction. *Advanced Materials*, 31(39):0193006, 2019.

[45] Ying Zhou, Carlos M Duque, Christian D Santangelo, and Ryan C Hayward. Biasing buckling direction in shape-programmable hydrogel sheets with through-thickness gradients. *Advanced Functional Materials*, 29(48):1905273, 2019.

[46] Menachem Stern, Viraaj Jayaram, and Arvind Murugan. Shaping the topology of folding pathways in mechanical systems. *Nature communications*, 9(1):1–8, 2018.

[47] Nathan C Keim, Joseph D Paulsen, Zorana Zeravcic, Srikanth Sastry, and Sidney R Nagel. Memory formation in matter. *Reviews of Modern Physics*, 91(3):035002, 2019.

[48] Marc Z Miskin, Kyle J Dorsey, Baris Bircan, Yimo Han, David A Muller, Paul L McEuen, and Itai Cohen. Graphene-based bimorphs for micron-sized, autonomous origami machines. *Proceedings of the National Academy of Sciences*, 115(3):466–470, 2018.

[49] Matthew B Pinson, Menachem Stern, Alexandra Carruthers Ferrero, Thomas A Witten, Elizabeth Chen, and Arvind Murugan. Self-folding origami at any energy scale. *Nat. Commun.*, 8:15477, 2017.

[50] Koryo Miura. Method of packaging and deployment of large membranes in space. *The Institute of Space and Astronautical Science report*, (618):1–9, 1985.

[51] Pascal Chossat, Debra Lewis, Juan-Pablo Ortega, and Tudor S. Ratiu. Bifurcation of relative equilibria in mechanical systems with symmetry. *Advances in Applied Mathematics*, 31(1):10–45, 2003.

[52] Farshad Khadivar, Ilaria Lauzana, and Aude Billard. Learning dynamical systems with bifurcations. *Robotics and Autonomous Systems*, 136:103700, 2021.

[53] Li Zhang and Gabor Stepan. Bifurcations in basic models of delayed force control. *Nonlinear Dynamics*, 99(1):99–108, 2020.

[54] Daniel Hexner, Nidhi Pashine, Andrea J Liu, and Sidney R Nagel. Effect of directed aging on nonlinear elasticity and memory formation in a material. *Physical Review Research*, 2(4):043231, 2020.

[55] Daniel Hexner, Andrea J Liu, and Sidney R Nagel. Periodic training of creeping solids. *Proceedings of the National Academy of Sciences*, 117(50):31690–31695, 2020.

[56] Tomohiro Tachi. Geometric considerations for the design of rigid origami structures. In *Proceedings of the International Association for Shell and Spatial Structures (IASS) Symposium*, volume 12, pages 458–460. Elsevier Ltd, 2010.

[57] See supplemental material at [url will be inserted by publisher] for [a pdf document of the single vertex origami pattern].

[58] See supplemental material at [url will be inserted by publisher] for [a pdf document of the double vertex origami pattern].